

Article

Smart Control System to Optimize Time of Use in a Solar-Assisted Air-Conditioning by Ejector for Residential Sector

Giovanna Avedian-González ^{1,†}, Apolinar González-Potes ^{1,2,†,*} , Vrani Ibarra-Junquera ^{2,†},
Walter A. Mata-López ^{1,†} and Carlos Escobar-del Pozo ^{1,†}

¹ Faculty of Electrical and Mechanical Engineering, University of Colima, Km. 9 Carretera Colima-Coquimatlán, Coquimatlán Col. C.P. 28400, Mexico; gavedian@uacol.mx (G.A.-G.); wmata@uacol.mx (W.A.M.-L.); cescobar@uacol.mx (C.E.-d.P.)

² Agrobio-Technological Laboratory, University of Colima Tecnoparque CLQ, Colima C.P. 28629, Mexico; vij@uacol.mx

* Correspondence: apogon@uacol.mx

† These authors contributed equally to this work.

Received: 25 January 2018; Accepted: 23 February 2018; Published: 28 February 2018

Abstract: The present work provides a series of theoretical improvements of a control strategy in order to optimize the time of use of solar air-conditioning by an ejector distributed in multiple solar collectors of vacuum tubes for the residential sector, which will allow us to reduce carbon-dioxide emissions, costs and electrical energy consumption. In a solar ejector cooling system, the instability of the solar source of energy causes an operational conflict between the solar thermal system and ejector cooling cycle. A fuzzy control structure for the supervisory ejector cycle and multi-collector control system is developed: the first control is applied to control the mass flow of the generator and the evaporator for different cooling capacities (3, 3.5, 4, 4.5 and 5 kW) and set a temperature reference according to the operating conditions; the second is applied to keep a constant temperature power source that feeds the low-grade ejector cooling cycle using R134aas refrigerant. For the present work, the temperature of the generator oscillates between 65 °C and 90 °C, a condenser temperature of 30 °C and an evaporator temperature of 10 °C. For the purpose of optimization, there are different levels of performance for time of use: the Mode 0 (economic) gives a performance of 17.55 h, Mode 5 (maximum cooling power) 14.86 h and variable mode (variable mode of capacities) 16.25 h, on average. Simulations are done in MATLAB-Simulink applying fuzzy logic for a mathematical model of the thermal balance. They are compared with two different types of solar radiation: real radiation and disturbed radiation.

Keywords: driven solar collector; fuzzy control; ejector cooling systems

1. Introduction

Mechanical vapor compression consumes exorbitant amounts of high-grade energy [1,2]. The high consumption of nonrenewable energy from fossil fuels, such as gas and oil, is a part of the remarkable deterioration of the planet, resulting in an increased temperature and higher rates of carbon-dioxide emissions (CO₂) [3–5]. Refrigeration and air-conditioning in buildings are among the reported highest consumers of energy, accounting for approximately 17% of the world's electricity consumption [6–8]. In order to reduce electricity consumption of air-conditioning, a solution would be the use of solar energy [9,10]. In Mexico, more than 70% of the territory has Global Horizontal Irradiation (GHI) values greater than 4.5 kWh/m². By taking advantage of this resource, interior comfort conditions will be enhanced with the use of solar-air-conditioning [9].

Solar thermally-driven heating systems work by thermal applications to absorb solar energy [11–13]. Solar collectors are used in this process to achieve a cooling task; however, usually, an auxiliary heater is needed to provide the required energy. The efficiency of a solar refrigeration system depends on the collector type, solar radiation intensity and the system operating conditions. When refrigeration systems operate at temperatures between 80 °C and 100 °C, a single glazed flat plate-type collector with a selective surface is recommended [14]. The vacuum tube [15] and parabolic solar concentrating collector [16] can provide higher thermal efficiencies at higher operating temperatures.

The cooling cycles operate by means of absorption, adsorption, Rankine, solar desiccant cooling cycles [17–20] and the ejector refrigeration system [21]. Desiccant cooling systems are used as isolated or as hybrid systems [22]. Absorption solar refrigeration systems commonly use ammonia-water as working fluids, which require high temperatures in the generator, provided by parabolic cylindrical collectors. Its use is mainly in refrigeration for food preservation and very little for air-conditioning systems. It is confirmed that absorption refrigeration systems that employ vacuum tube solar collectors are more efficient than those that use flat solar collectors [23]. The absorption refrigeration system uses a process of chemical absorption; therefore, its design is complicated. In addition, the high installation cost delays its application in solar cooling systems [24].

Ejection cooling is a system in which the refrigeration effect is produced through a phase change and which is analyzed in this work. In the ejection systems, the compression that the refrigerating fluid must suffer to produce cooling does not take place in a compressor as in the absorption systems. The pressure of the fluid is increased by an exchange of kinetic energy in an ejector. This method of compression does not involve moving parts and therefore does not consume energy. However, the compressor of the ideal vapor-compression refrigerator cycle is a substitute for an ejector and a pump (at least one). Ejector cooling is one of the most promising technologies because of its relative simplicity and low capital cost when compared with other heat-driven refrigeration systems such as vapor absorption [25]. The relatively low cost of the ejector in the air-conditioning system makes it possible to be used in the residential sector, and it can be used as an environmentally-friendly refrigerator operating with a low boiling point [24]. Cooling cycles per ejector are trithermic; the exchange heat comes from three different temperatures: evaporator, in which the heat is collected from the cold area; generator, which has the hottest temperatures from solar collectors; and condenser, which releases energy to the environment [26]. However, in solar ejector cooling systems, the instability of solar power and the thermal refrigeration cycle requires great complexity to operate and control the complete cycle. This work proposes a system of control integrated with an optimization system to improve this.

The main idea of the present work is to develop an intelligent control system for better use of multiple solar collectors of vacuum tubes for solar air-conditioning applications by an ejector. This system requires a constant temperature source of energy for the process, which should be independent of weather conditions and shade. This controller follows a temperature reference, which is fixed by another governor control, with the objective of optimizing the use of time, taking into account the operation of the ejector-based refrigeration cycle, which will take advantage of the physical resources and will minimize the costs of operation and maintenance. These systems are difficult to control due to certain factors such as the nonlinear solar thermal characteristic and perturbations, in which the system is subjected to energy and the changes that arise in the dynamics of the process over time and optimal operating conditions of the refrigeration cycle. The results obtained contribute to those achieved by the classical control methods. We develop an intelligent control system based on fuzzy logic, for the synthesis of a nonlinear dynamic system model integrated with the operation of a refrigeration cycle. This research is the basis for future studies; however, the efficiency of the ejector cooling system should be further improved to compete with the absorption system [24].

The outline of this paper is as follows. Section 2 presents an overview of related works, such as other performance and comparative studies. In Section 3, a description of a solar air-conditioning

system, with different constituent elements, is presented. Section 4 discusses and analyzes a fuzzy control structure to operate and control the complete refrigeration cycle. In Section 5, a performance analysis to optimize the refrigeration cycle is presented; at the same time, the validation results and discussions of the simulation are carried out. Section 6 concludes this study.

2. Related Works

In this paper, we address various aspects to optimize the time of use for an ejector cooling cycle using an intelligent control, which includes aspects such as control of multiple vacuum tube solar collectors, thermal cooling cycle analysis, control of temperature energy source, in spite of unknown dynamics and perturbations, and selection of functioning modes by end users with the same controller. To meet these requirements, the main focus is the optimization of an intelligent control system for a better time of use in a solar-assisted air-conditioning by an ejector. In this section, we provide a discussion of the related literature.

A control strategy to improve the partial load performance of the solar air-conditioning system was applied by [27,28]; due to the nocturnal unavailability of solar energy, studies have been carried out to improve the performance of solar air-conditioning by means of thermal storage. Advanced automation and control for buildings are possible in order to lower the consumption of energy, where improved control strategies of building systems have shown a decrease of overall energy consumption [29]. In [30], the authors present a method of designing a nonlinear predictive controller based on the Takagi–Sugeno fuzzy model, using the internal model control scheme to compensate for disturbances and modeling errors; the algorithm is applied to temperature control in an air-conditioning system. Hot water at 65 °C is supplied to the coil, which exchanges the heat between the hot water and the surrounding air. A model-based predictive control of a solar thermal system consisting of a flat plate solar collector and heat exchanger was described in [29].

The aim is to control the temperature at the outputs of the heat exchanger in the solar circuit, as well as the storage circuit using a model-based predictive control, where the desired set-points for the temperature should be achieved predictively consuming the minimum energy, whereas variations such as solar radiation, ambient temperature, etc., should be rejected. The vector $u(K)$ contains the mass flow rates used as the control variables for temperature control. The optimization routine was implemented using the MATLAB optimization toolbox. The model predictive controller shows a behavior with a much lower demand on control energy compared with the PI controller and good performance with regards to disturbance rejections. According to [31], a predictive control for solar absorption cooling systems has the objective of optimizing the use of the solar energy, in order to ensure the cooling requirement of the building; a relaxation technique also is proposed to solve the nonlinear hybrid problem. The aim is to optimize the energy consumption, comfort and lifetime of the system by better interactions, in order to define the temperature profile in the building and the hot water consumption flow rate.

In [32], a sliding mode predictive control is presented in a way that is combined with model-based predictive control; mixing both control techniques results in a new predictive control with better robustness properties, producing disturbances by changes in solar irradiation and the solar collector's inlet temperature. It consists of a solar field that produces hot water with an absorption machine, achieving a cooling power of 35 kW. Its output temperature can be controlled by adjusting the water flow inside the solar field by manipulating the B1 pump speed. Pursuant to [33], the employment of a model-based predictive control algorithm for the energy-efficient temperature control of a solar-thermal system consists of a solar collector and heat exchanger; the model predictive control strategy showed good performance with regards to disturbance rejections.

In [34], a supervisory control is implemented in a solar air-conditioning plant, where the control goal was to match the cooling demand and, at the same time, minimize the gas heater contribution to the absorption chiller heat input, thus showing the importance of the system models for the robustness of this control. According to [35], a modeling and control strategy for a novel HVAC system

is presented in a way that considers temperature, humidity ratio and CO₂ concentration; the HVAC system is Multi-Input Multi-Output (MIMO); thus, a dynamic extension algorithm can be employed, and a feedback linearization technique is applied. A Linear-Quadratic Regulator (LQR) is designed to optimize control performance and to stabilize the proposed HVAC system.

All of these works propose control solutions with additional systems that supply energy, mainly with an auxiliary generator. On the other hand, the technique based on ejector cooling is not generally considered; in this work, we have presented the advantages of using the ejector for use in air-conditioning systems in residential areas. In this paper, we propose a control model, which according to different parameters such as operation modes set by end users, solar radiation disturbances and optimal conditions of operation of the ejector cooling cycle, sets the reference temperature of storage tank and references in the mass flows of operation for the generator and evaporator, thus optimizing the time of use of air-conditioning operated by the ejector without the need of energy supply by an alternate source.

Recent studies on the temperature required for the ejection cooling cycle are mentioned in this work. In [36], the authors report a maximum cooling capacity and COP using a generator temperature of 90 °C and 92.8 °C. According to [37], an experimental investigation on ejector cooling at low temperature is realized by obtaining a COP of 0.42 at a generator temperature of 74 °C, evaporator temperature of 10 °C and a critical condenser temperature of 29 °C. A cooling capacity of 1080 W was obtained for an area of 9.2 m² of single-glazed selective-type collectors in a horizontal position. In [38], the ejector performance using R141brefrigerant with thermal storage for solar air-conditioning is presented. A COP average of 0.265 is given for an area of 10 m² of an evacuated solar collector at a generator temperature of 84 °C, condenser temperature of 28 °C and evaporator temperature of 8 °C for a cooling capacity of 3.5 kW.

According to [24], a solar ejector cooling system is developed using R141b refrigerant; a COP of 0.5 is obtained experimentally for a single-stage ejector cooling system at a T_g of 90 °C, T_c of 28 °C and T_e of 8 °C, covering a cooling capacity of 10.5 kW for a solar flat-plate collector area of 68 m². As presented in [39], an acceptable coefficient of performance is one for which generator temperatures should not fall below 90 °C, evaporator temperatures below 10 °C and condenser temperatures be over 35 °C; the COP was 0.13 for an evacuated tube area of 50 m², which can provide a cooling capacity of 3.5 kW; T_e below 10 °C resulted in poor system performance. In [40], an ejector cooling system using water as a working fluid is not suitable for low evaporator temperatures; the COP ejector decreases rapidly as the T_c increases. The results indicated that both COP and system efficiency increased with generator temperature. According to [41], R141b is used as a working fluid to verify the theoretical results.

As for thermal analysis in the previous works, the biggest difference with our work is to maintain a low operating range in the generator temperature, which oscillates between 65 °C and 90 °C; the condenser temperature is 30 °C, and the evaporator temperature is 10 °C.

3. Description of the Solar Air-Conditioning Plant

The solar air-conditioning system consists of two parts, the energy source and the ejector cooling cycle, and the structure of the solar thermal system is shown in Figure 1 with its respective controlled variables. In the first, a mathematical model is presented to describe the solar thermal system of vacuum tubes; the interest is to build a mathematical model that is able to scale and integrate with the refrigeration cycle and additionally contribute with rapid prototyping to optimize the time of use of the air-conditioning, thus integrating all aspects related to the intelligent control system. The second consists of the cooling cycle, in which a series of theoretical analyses was carried out to verify at which points of the generator temperature the ejector can operate; according to the different cooling capacities in which it operates, it will have a respective amount of mass flow \dot{m} .

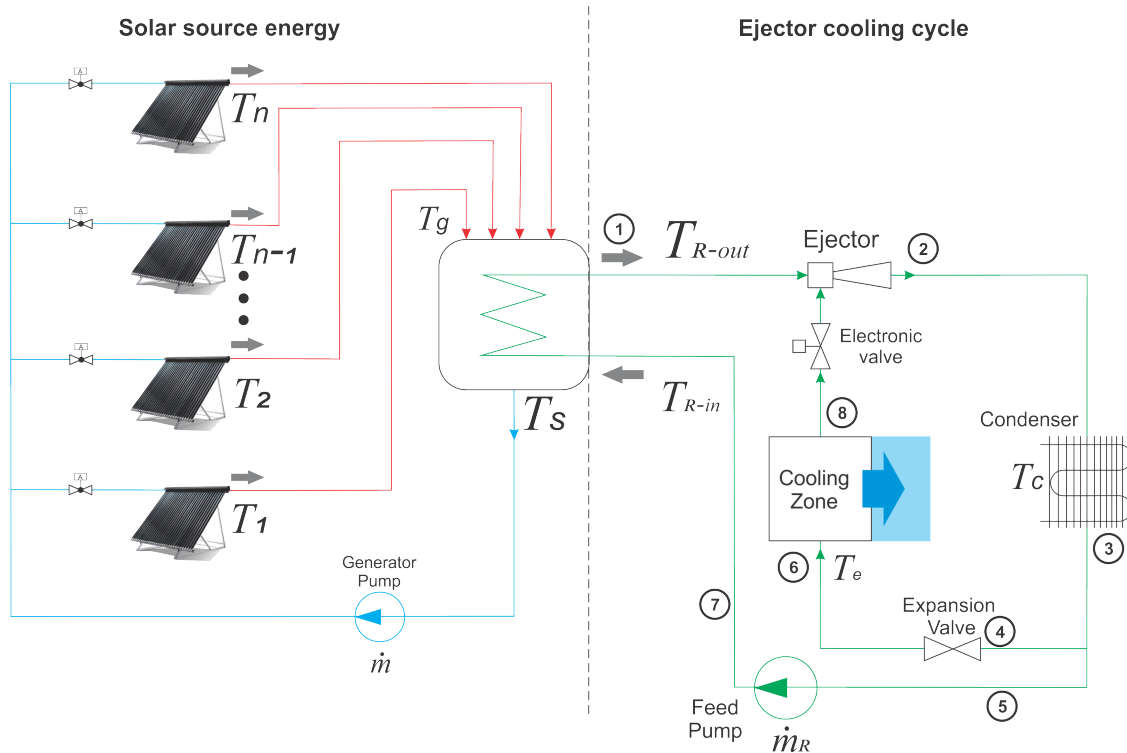


Figure 1. Structure of the solar thermal system of vacuum tubes.

The dynamic system of the solar source energy is represented by the variable to be controlled, which is the mass flow \dot{m} in each solar collector; this will provide the constant energy source. The present model allows us to study the effect that the manipulated variable of closed-loop control \dot{m} and the perturbations (solar radiation) have on the variable of interest T_g . The fuzzy controller aims to control the input temperature to the generator T_g to be constant, where T_1, T_2, \dots, T_n are the temperatures of each solar collector. The analysis applies to four solar collectors with 30 vacuum tubes for each one, a tank dimensioned to a capacity of 180 liters, an evaporator temperature of 10 °C and a condenser temperature of 30 °C. However, this model can be variable, depending on the required cooling capacities.

The ejector cooling cycle operates using low-grade thermal energy produced in the heat exchanger, as mentioned earlier in the solar energy source section. The cycle function is such that the portion of the expenditure being driven through the generator undergoes a direct thermodynamic cycle, which allows the rest of the mass flow of the refrigerant to complete the inverse thermodynamic cycle of a refrigeration machine. Pressurization starts from the conversion of kinetic energy into enthalpy by means of a diffuser; thus, it is necessary to induce kinetic energy to the refrigerant flow, which is a process that takes advantage of the Venturi effect provided by an ejector (nozzle-inductor-diffuser set) [26]. The main disadvantages of this system are its low Coefficient Of Performance (COP), which varies in the range of (0.1–0.4), and its operation must be around critical points; otherwise, its COP deteriorates rapidly [42]. The present research does not model the thermal performance of the ejector cooling cycle; instead of that characteristic temperature, flow rates and COP of the ejector cycle obtained from different authors are used (values are shown in Table 1).

Table 1. Low operating temperatures of an ejector.

T_g (°C)	T_c (°C)	T_e (°C)	kW	Working Fluid	COP	Reference
50–60	26.5–38.5	8–16	1.8–3	R134a	0.3–0.48	[43]
65–85	25–40	6–10	-	R134a	0.355	[44]
60–85	25	–5–5	-	R717	0.06–0.34	[45]
40–70	15–40	10–15	0.5–1.1	water	0.1–1.2	[46]
65–90	26–38	2–13	0.5	R134a	0.09–0.16	[47]

A COP of 0.48 will be used in this work according to experimental studies of the refrigeration cycle by ejector with R134a refrigerant [43]. R134a gives better performance and a higher critical entrainment ratio in comparison with other refrigerants, which will be used for the present research [48]. The present investigation is carried out to cool approximately an area of 20–25 m² in different cooling capacities. The properties of the refrigeration cycle are listed according to Figure 1. Table 2 shows the temperatures at each point of the operation of the refrigeration cycle, with its respective pressure, enthalpy and phase state. The data were obtained from thermodynamic tables of the R134a refrigerant [49].

Table 2. Cooling cycle properties.

Number	Temperature (°C)	Enthalpy (kJ/kg)	Pressure (MPa)	Phase Status
1	65	279.64	1.891	Saturated vapor
3, 4, 5	30	93.58	0.77064	Saturated liquid
6	10	$h_6 = h_4 = h_3$	0.41489	Liquid-vapor
7	30.7	94.5235	$p_7 = p_1$	Subcooled liquid
8	10	256.16	$p_8 = p_6$	Saturated liquid

4. Fuzzy Control Structure for Supervisory Ejector Cycle and Multi-Solar Collector Systems

Solar air-conditioning systems require optimal operating conditions to secure the highly demanding indoor temperature. This section describes the implemented fuzzy control. The nonlinearities, imprecisions, variations, more than one control and the manipulated variables presented in this plant make the controller design a nontrivial task.

Fuzzy logic has the ability to transform vague information and expert knowledge into numerical computable data, thus allowing control of plants with the aforementioned characteristics. In this section, we describe the implemented fuzzy control. The control structure is represented in two layers, as shown in Figure 2. Layer 1 is the fuzzy control of the solar collector system; the aim of Layer 1 is to control the temperature at the outputs of the heat exchanger in the solar circuit, as well as storage circuit using model-based fuzzy logic control. Layer 2 is the supervisory fuzzy control of the ejector cooling cycle, which according to different parameters such as operation modes, solar radiation disturbances and optimal conditions of operation of the ejector cooling cycle, sets the reference temperature of storage tank and the references in the mass flows of operation for the generator and evaporator. The supervisory or governor controller uses Servo-Pumps (SP) and Servo-Electronic-Valves (SEEV) as actuators for the evaporator and generator flow.

with regard to time [50]. This dynamic equation is maintained as a function of the working fluid mass flow \dot{m} of each solar collector, considering constant properties as the density $\rho_f = 998.2 \text{ kg/m}^3$, specific heat $C_{pf} = 4182 \text{ J/kg K}$ and the tank volume $\forall_T = 0.180 \text{ m}^3$. This equation also considers the energy requirements of the refrigeration cycle, $T_{R_{out}}$, which use R134a as the refrigerant fluid with a mass flow of $\dot{m}_R = 0.0567 \text{ kg/s}$ and specific heat of $C_{PR} = 1443 \text{ J/kg K}$:

$$\frac{dT_s}{dt} = \frac{\dot{m}_1 T_1 + \dot{m}_2 T_2 \dots \dot{m}_n T_n}{P_f \forall_T} - \frac{(\dot{m}_1 + \dot{m}_2 \dots \dot{m}_n) T_S}{P_f \forall_T} - \frac{\dot{m}_R C_{PR}}{P_f \forall_T C_{pf}} (T_{R_{out}} - T_{R_{in}}). \tag{1}$$

To provide the thermal energy to the generator, an arrangement of vacuum tube solar collectors is required. These collectors consist of a heat pipe inside a vacuum-sealed tube and have shown that the combination of a selective surface and an effective convection suppressor can lead to good performance at high temperatures. The vacuum envelope reduces convection and conduction losses, so that the collectors can run at higher temperatures than the flat plate [51].

For the analysis, the solar collectors are divided into two thermal systems: the vacuum tubes and the storage tank. Equation (2) expresses the energy balance of the storage tank, taking into account that the tank walls are adiabatic, where T_S represents the output temperature of the generator, T_T is the output temperature of the tank, T_a is the temperature of the vacuum tubes, N is the total number of vacuum tubes in each solar collector, (\dot{m}_{conv}) is the natural convection mass flow rate and $M_t = 292.6345 \text{ kg}$, which is the mass of water in the tank:

$$\frac{dT_T}{dt} = [(\dot{m} (T_S - T_T)) + (N \cdot \dot{m}_{conv} (T_a - T_T))] \frac{1}{M_t}. \tag{2}$$

The differential Equation (3) shows the energy balance of water inside the tubes, considering heat losses by radiation to the atmosphere. For simulation purposes, two types of solar radiation G_t are compared: the first reaches 900 kW/m^2 , which is obtained from real data in seconds of a solar radiation of a normal sunny day of the state of Colima (Pacific center zone of the Mexican Republic), and the second, which is considered as perturbation by its low solar radiation of 500 kW/m^2 and is realized by means of a sinusoidal equation, as represented in Equation (4):

$$\frac{dT_a}{dt} = \left[(G(t) (\tau\alpha) A_{pint}) + (\dot{m}_{conv} C_{pf} (T_T - T_a)) - (\sigma \epsilon_{gp} A_{pint} (T_a^4 - T_{sky})) \right] \frac{1}{C_f}, \tag{3}$$

$$G_t = \frac{500}{2} \times (\sin(\Omega \times t) + abs(\sin(\Omega \times t))) \tag{4}$$

The input variables for the fuzzy controller are the error defined as the difference between the desired value of temperature in tank (T_{ref}) and the actual value T_s , while dT_s/dt act as the derivative of temperature T_s and T_c is the temperature in the solar collectors and allows one to know the behavior of solar radiation at all times.

The following six fuzzy sets, L (Large), M (Medium), H (High), NH (High Negative), Zero (Zero) and PH (High Positive), represented as triangular and trapezoidal functions of the membership degrees, are defined for each of the input variables. Output temperature in collectors, derivative temperature and temperature error in the tank are quantified according to the memberships in the fuzzy sets, as shown in Figure 4. Figure 4a shows the input for collector temperature and uses the following fuzzy sets: L (Large), M (Medium) and H (High). Figure 4b shows the input for derivative temperature in the storage tank, NH (High Negative), zero (Zero) and PH (High Positive), and Figure 4b is the input for storage tank temperature: NH (high negative), Z (Zero) and PH (High Positive). Finally, Figure 5 shows the output fuzzy set membership function for flow reference in each collector, using the following fuzzy set: Zero (Zero), P (Positive) and G (Good).

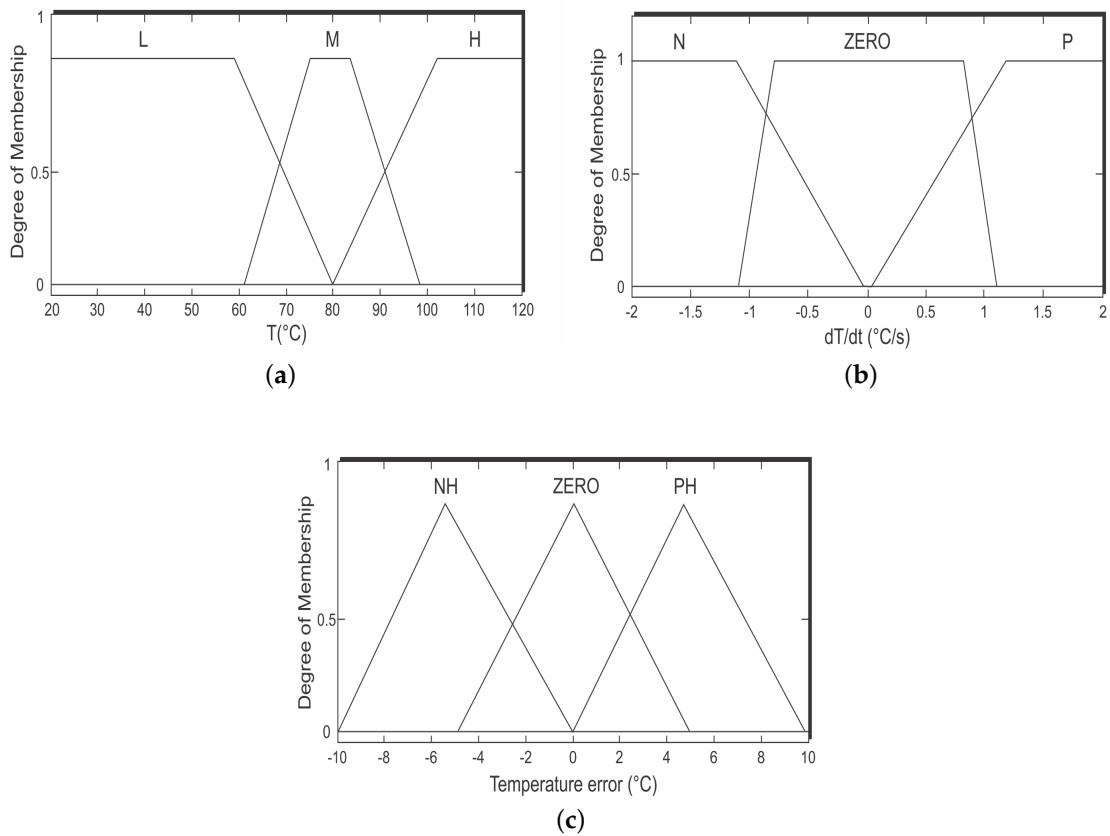


Figure 4. Input fuzzy set membership function for Layer 1: (a) input for collector temperature; (b) input for derivative temperature in the storage tank; (c) input error (reference -current temperature) for the storage tank. L, Large; M, Medium; H, High; NH, High Negative; PH, High Positive.

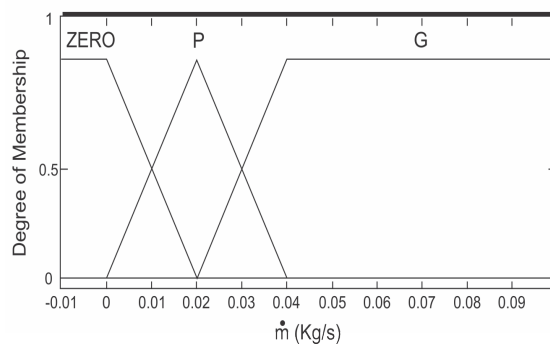


Figure 5. Output fuzzy set membership function for the flow reference in each collector. P, Positive; G, Good.

4.2. Layer 2: Supervisory Fuzzy Control of Ejector Cooling Cycle

Layer 2 is a supervisory controller, which will be controlled according to the different modes of operation implemented. This layer will be subject to the temperature variable of the solar collectors T_{col} , which will be a function of the disturbances of solar radiation G . Depending on T_{col} and G , a reference in the generator mass flow \dot{m}_g and the evaporator mass flow \dot{m}_e are given. The temperature reference T_{ref} Layer 2 is connected to Layer 1. A supervisory or governor controller uses Servo-Pumps (SP) and Servo-Electronic-Valves (SEEV) as actuators for the evaporator and generator flow. The operating

modes are defined as an input to the system, according to the conditions of use that the operator or end user requires. The operating modes are defined continuously from 0–5. Mode 0 represents the highest energy consumption savings, and Mode 5 has the highest power consumption, but higher cooling power. The operator or end user according to his or her needs defines the mode of operation; however, the supervisory or optimization layer, based on additional operating conditions such as disturbances and climatic conditions, defines optimal references for a longer time of use of solar air-conditioning.

The supervisory controller treats a set of information to optimize the operating conditions of the complete cooling cycle. The temperature in solar collectors, temperature variation in solar collectors and temperature in tank storage and operation modes are the inputs to the multiple input and multiple output plant. Temperature and its variation in solar collectors give the solar energy currently available. The controller outputs are the reference temperature for the tank (reference for Layer 1), mass flow references for the servo-pump controlling the flow of the generator and the servo-valve controlling the flow of the evaporator, to make the ejector operate at a critical or noncritical double-choking condition obtain better performance or effective time of use of the air-conditioning system.

For the control simulations, the temperature conditions set T_g was 10 °C higher than the coolant outlet temperature [24], $T_{R_{out}} = T_g - 10$ °C; the coolant inlet temperature $T_{R_{in}} = 30.7$ °C, the condenser temperature $T_c = 30$ °C and the evaporator temperature $T_e = 10$ °C. For the present investigation, the temperature range of the generator is defined as 55–90 °C, in relation to Table 1, to determine the operating points of the ejector.

Figure 6 shows the entrainment ratio with respect to the different temperatures of the generator, where, at 75 °C, the optimum operating point is located, according to our objective to optimize the air-conditioning use time; 65 °C is defined as the minimum temperature of the generator at which the ejector can operate, considering there is a loss of 10 °C. The behavior of the entrainment ratio at different condenser temperatures is presented in Figure 7; it can be appreciated that the condenser temperature must be maintained at 30 °C, due to the generator’s minimum temperature of 65 °C, which depends on an entrainment ratio of 0.54654, according to Figure 6.

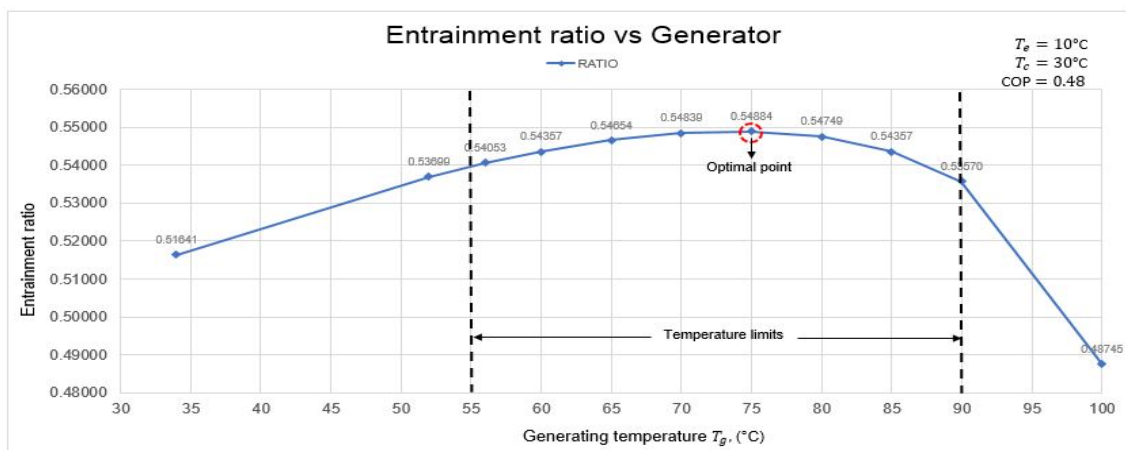


Figure 6. Entrainment ratio with respect to the generator temperature.

Equation (5) determines the thermal load (Q_R) required for the cooling area. According to our objective, which is to optimize the use of the refrigeration cycle, different cooling capacities, e.g., 3.0, 3.5, 4.0, 4.5 and 5 kW, are maintained for our analysis. Equation (5) helps us to calculate the necessary energy and mass flow to operate the ejector refrigeration cycle for different cooling capacities:

$$Q_R = \dot{m}_e(h_8 - h_6). \tag{5}$$

For the development of the control strategy, it is necessary to calculate the mass flow rate of the evaporator and the generator for different powers. In relation to the analysis performed for the

five cooling capacities, obtained according to Figure 8, the mass flow rates of the evaporator will remain constant in each cooling capacity, according to the temperature limit of the generator. For the generator mass flow, Figure 9 shows that the flow varies in each of the different cooling capacities.

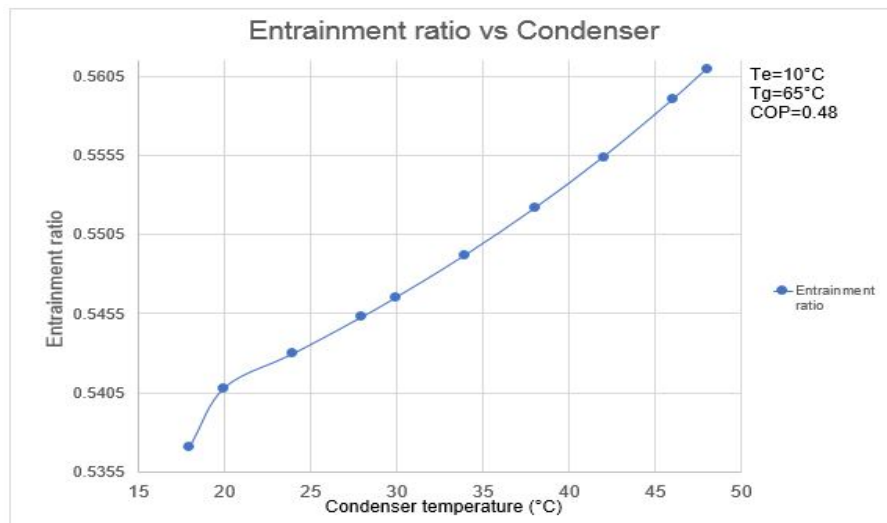


Figure 7. Entrainment ratio with respect to the temperature of condenser.

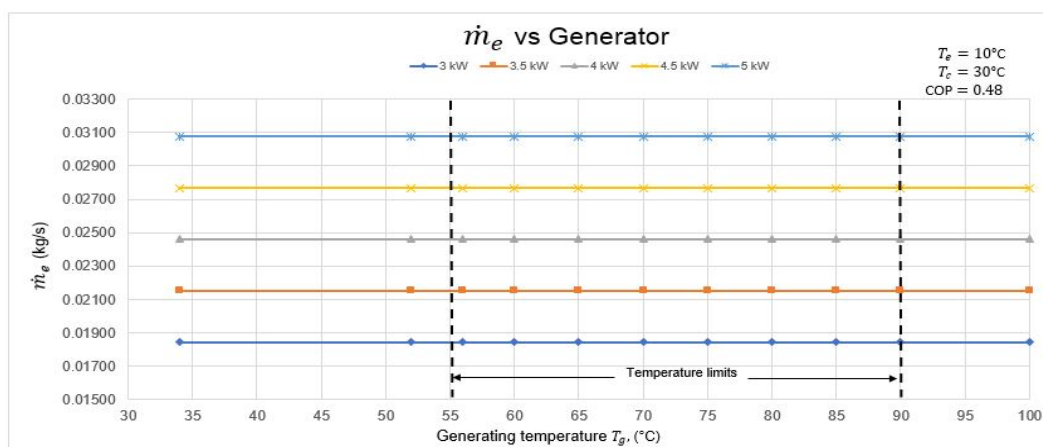


Figure 8. Mass flow of the evaporator (\dot{m}_e) considering five powers (kW).

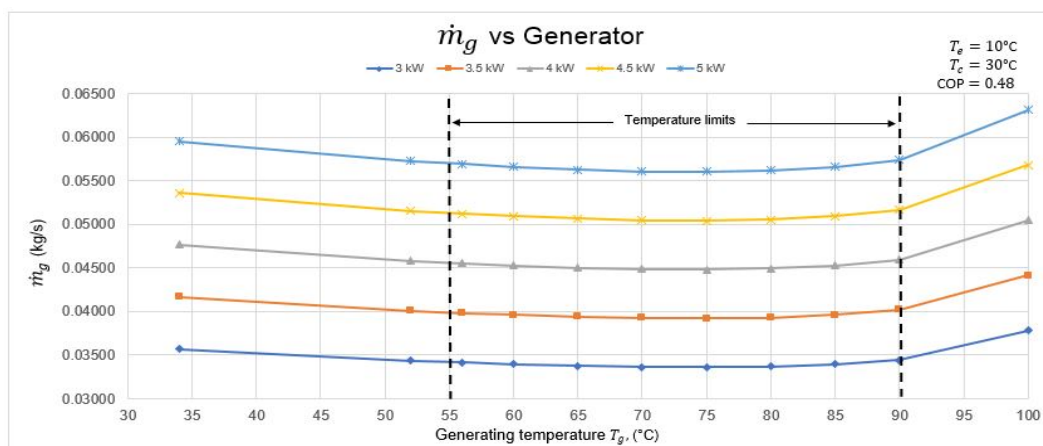


Figure 9. Mass flow of the generator (\dot{m}_g) considering five powers (kW).

To facilitate the control strategy, we proceed to calculate the average mass flow of the evaporator and the generator with the five cooling powers. Figure 10 and Table 3 show the linkage of the mass flows.

Table 3. Average of \dot{m}_e and \dot{m}_g for different cooling powers.

Cooling Power (kW)	\dot{m}_e (kg/s)	\dot{m}_g (kg/s)
3	0.01845	0.03382
3.5	0.02153	0.03946
4	0.02460	0.04510
4.5	0.02768	0.05073
5	0.03075	0.05637

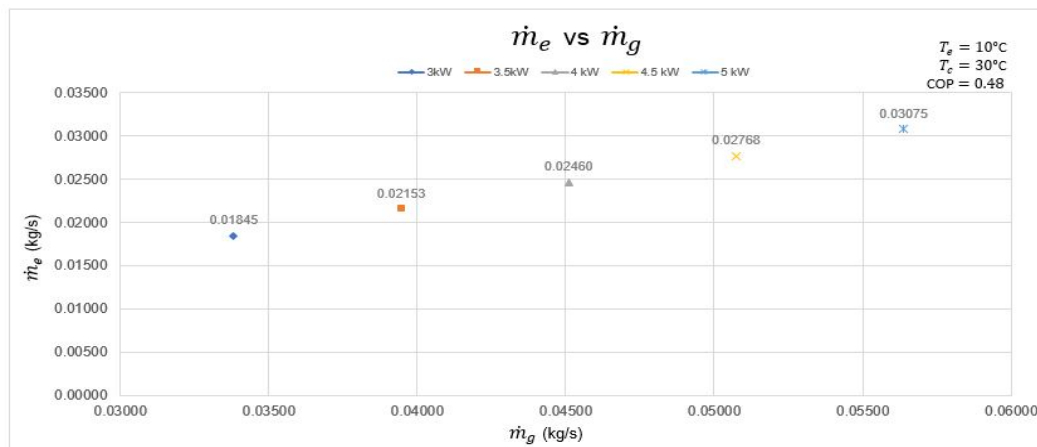


Figure 10. Mass flow of the generator (\dot{m}_g) and evaporator (\dot{m}_e) considering five different powers (kW).

The operation modes are determined by the end user. Mode 0 means economical use in energy; according to the analysis made in the previous section, the reference for the tank temperature control system should be low, and the outputs of references in flow generator and evaporator also should be moderately low, but within the limits that have been set for the ejector cooling cycle to work. In contrast, Mode 5 must set the reference temperature for the tank control to the maximum permissible by the previous analysis performed.

Figure 11 shows the input variables for the fuzzy governor controller; this variable is the actual value T_c , while dT_c/dt act as the derivative of temperature T_c in the solar collectors and allow one to know the behavior of solar radiation at all times. Finally, in Figure 12 are shown the governor outputs \dot{m}_g and reference temperature for fuzzy control of the solar collector.

The following fifteen fuzzy sets: LL (Low Low), L (Low), M (Medium), H (High), HH (High High), NH (High Negative), NM (Medium Negative), Z (Zero), P (Positive), PH (High Positive), M_1 (Mode 1), M_2 (Mode 2), M_3 (Mode 3), M_4 (Mode 4) and M_5 (Mode 5), represented as triangular and trapezoidal functions of the membership degrees, are defined for each of the input variables; see Figure 11. Output fuzzy set membership function for generator mass flow and input temperature reference to fuzzy control of solar collector, respectively, use the following fuzzy sets: Mg_1 (Generator Mass Flow 1), Mg_2 (Generator Mass Flow 2), Mg_3 (Generator Mass Flow 3), Mg_4 (Generator Mass Flow 4), and Mg_5 (Generator Mass Flow 5) and output temperature set reference for fuzzy control of solar collector: LL (Low Low), L (Low), M (Medium), H (High) and HH (High High); see Figure 12.

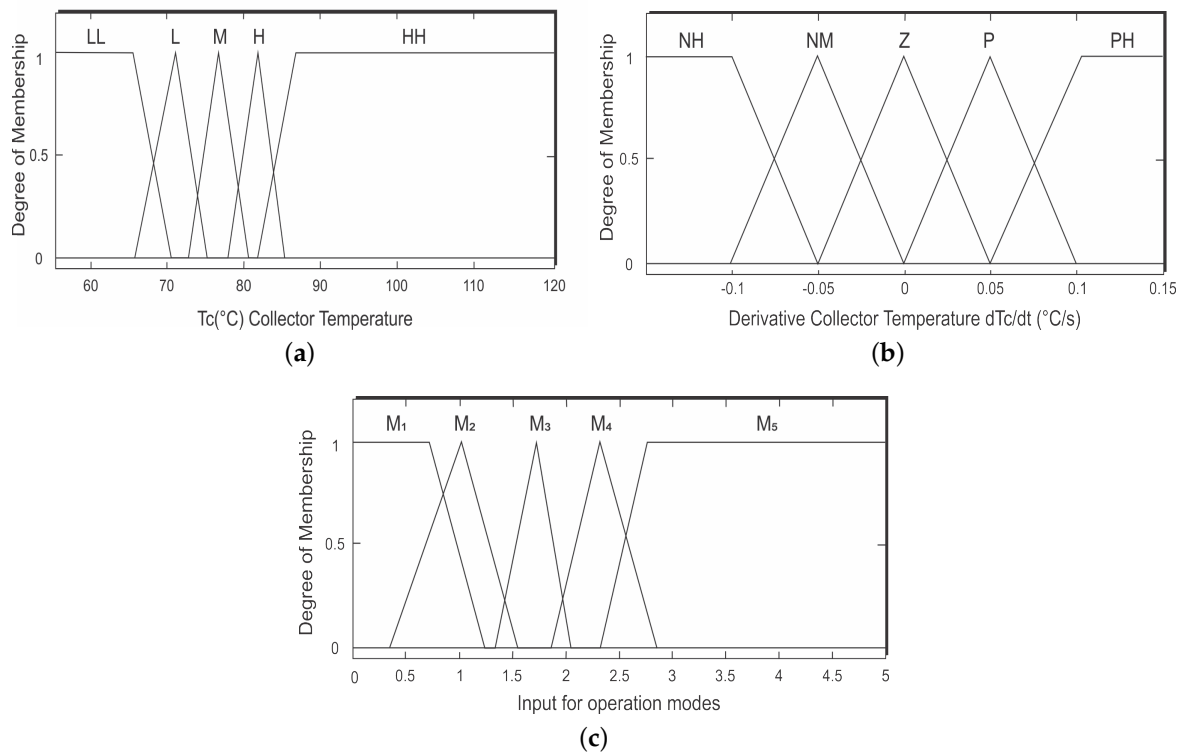


Figure 11. Fuzzy input variables for supervisory control. (a) Input for collector temperature; (b) input for derivative collector temperature; (c) operation modes. LL, Low Low; HH, High High; Z, Zero; NM, Medium Negative.

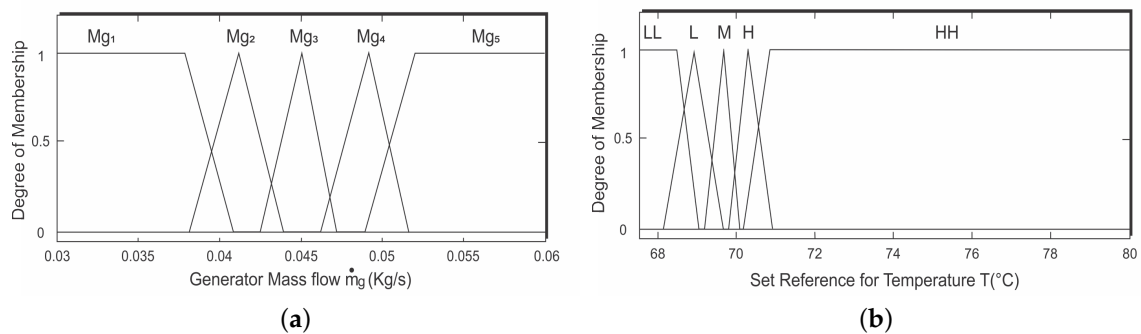


Figure 12. Output fuzzy set membership function for generator mass flow and input temperature reference to the fuzzy control of solar collector, respectively. (a) Output set reference for generator mass flow; (b) output set reference for temperature for fuzzy control of solar collector.

5. Evaluation, Results and Discussion

In this work, we are interested in the performance analysis of multiple control of driven-solar collector systems for a solar-ejector air-conditioning system. The main idea is to optimize the refrigeration cycle in a solar air-conditioning system, using a single controller, optimizing physical resources and minimizing operating and maintenance costs. One of the main reasons is to offer greater scalability, thus facilitating different operation points in an ejector-based refrigeration cycle, without the need for reconfiguring the system, while maintaining functional restrictions in the system.

The priority is to increase the times of use of a solar air-conditioning system, facilitating their implementation, maintenance and easy development. In this context, a control structure based on a system of supervision or a governor and a system of regulations based on fuzzy logic have been implemented. The simulation time considered for the performance analysis of the system is a day, taking into account that this time is enough to carry out a full solar air-conditioning system procedures. In subsequent analyses, the time (86,400 s) used for the simulation also allows us to appreciate the behavior of the control and the entire system as a whole against perturbations.

The simulations are performed for two types of solar radiation, the first with real solar radiation and the second with a low radiation of 500 kW/m^2 . The first is executed with real solar radiation of a normal day of the state of Colima in seconds, which starts from 7:00 a.m. and ends around 5:30 p.m. (winter time), as shown in Figure 13a,b. To show the behavior of the implemented control system and the optimization of cooling time, three simulations with different modes of operation of the air-conditioner are analyzed; the first mode of operation called Mode 0 is the most economical; the second mode of operation called Mode 5 is the least economical, but has higher cooling power; and finally, a variable mode is realized, whose capacities of refrigeration vary according to the solar radiation.

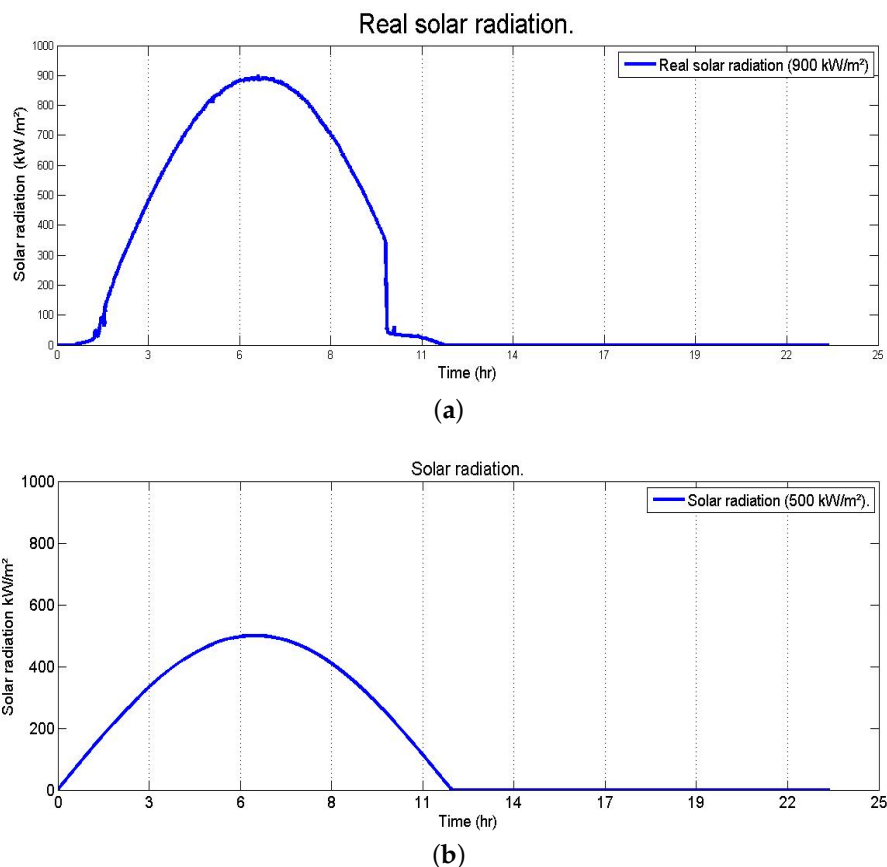


Figure 13. (a) Real solar radiation of a normal day of the state of Colima in seconds; (b) solar radiation of 500 kW/m^2 , which is considered as low radiation. (a) Real solar radiation; (b) solar radiation of 500 kW/m^2 .

5.1. Real Solar Radiation

The first test is for Mode 0, according to Figure 14a; the collector reaches a temperature higher than $110 \text{ }^\circ\text{C}$, and the reference is kept constant at a low temperature of $68 \text{ }^\circ\text{C}$, which allows us to have a greater use of cooling, but with low power. On the other hand, Mode 5 is shown in Figure 14b, reaching a collector temperature of $110 \text{ }^\circ\text{C}$; due to the user's needs for more cooling power, a higher

reference temperature of 75 °C is required, which leads to decreasing the use time. For Modes 0 and 5, the cooling capacities are shown in Figure 15. For Mode 0, a capacity of 3 kW is needed, which remains in the lowest capacity because it is the most economical system. For Mode 5, its cooling capacity is 5 kW because it is the mode that requires more power. The mass flow of the generator and evaporator for Modes 0 and 5 are shown in Table 4 and Figure 16.

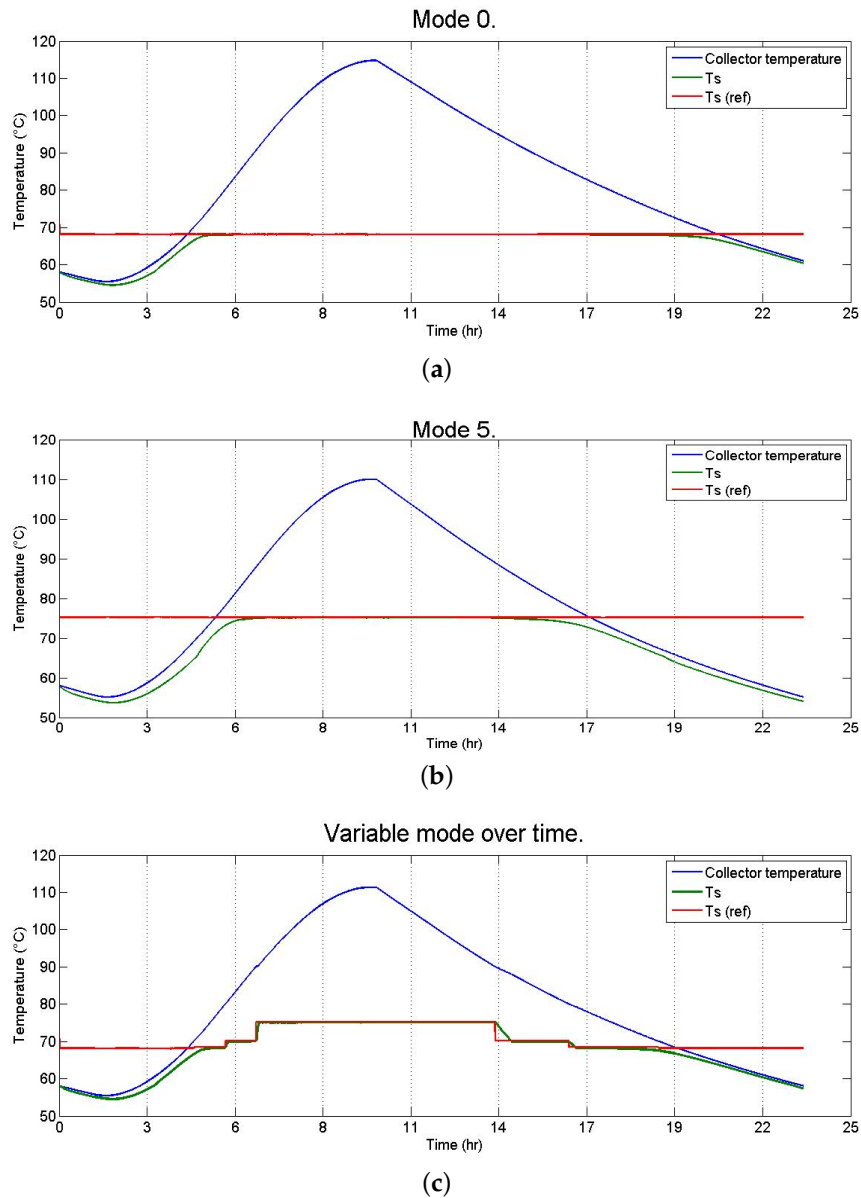


Figure 14. In the numerical simulation, blue lines represent the collector temperature, green solid lines the response of temperature for storage tank and red solid lines the temperature reference. (a,b) Temperature reference is constant; (c) different mode changes applied over time.

Table 4. Comparison of the economic mode and the maximum mode for a radiation of 900 kW/m².

Mode of Use	Power (kW)	Mass Flow \dot{m}_g (kg/s)	Mass Flow \dot{m}_e (kg/s)	Time (h)
Economic mode (Mode 0)	3	0.035	0.018	17.55
Maximum mode (Mode 5)	5	0.0548–0.0553	0.0299–0.0301	14.85

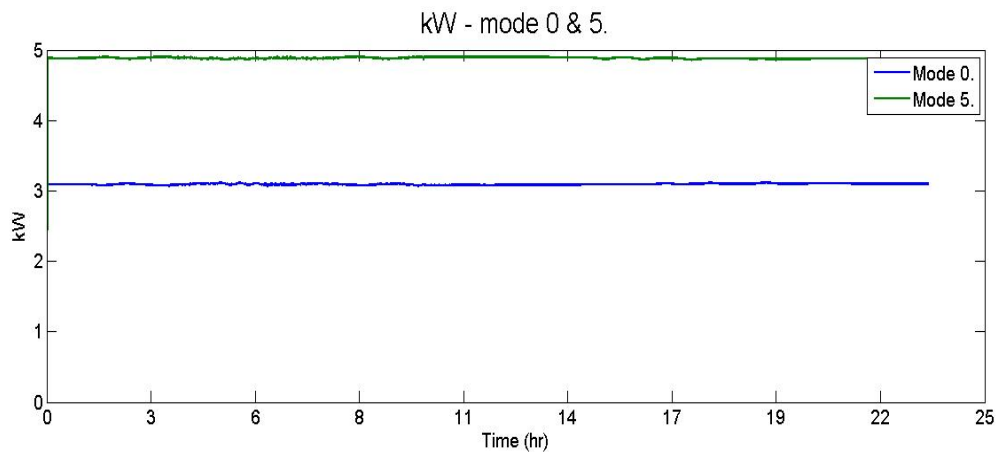


Figure 15. Cooling capacity for Modes 0 and 5.

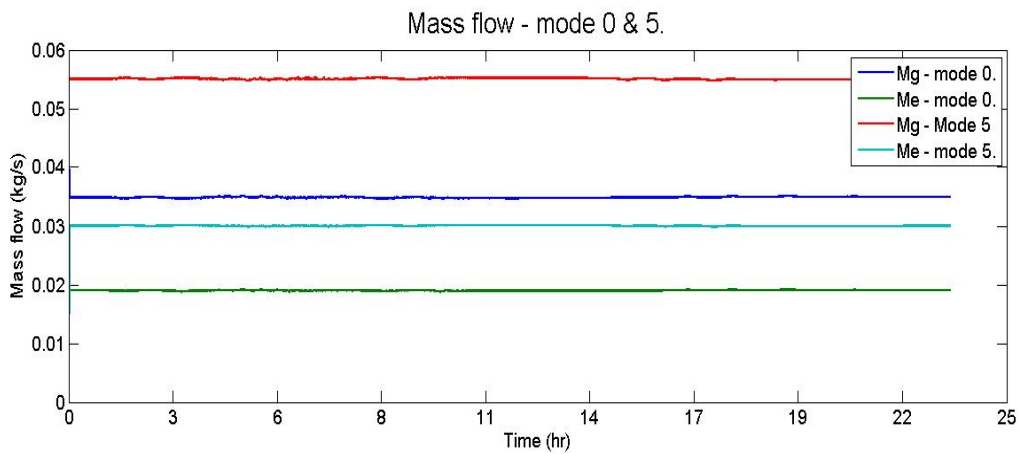


Figure 16. Mass flow of the generator and evaporator in Modes 0 and 5.

The last mode of operation, called variable mode, reaches a collector temperature of 112 °C, and the reference varies at three different temperatures: starting with 68 °C, after 5 h, it reaches 70 °C; passing 1.38 h, it reaches 75 °C; after 14 h, the reference temperature drops from 75–70 °C; after 2 h, the reference drops back from 70–68 °C. This is the behavior of variable mode, which is regulated according to the solar radiation, as shown in Figure 14c.

Figure 17a shows a simulation with different modes of operation varying in time, which is a situation dependent on the operator of the solar air-conditioning system. The variation of variable mode is shown in Figure 17a, where the modes operate from 0–5. The controller optimizes the time of use according to the climatic conditions and solar radiation. Different powers and mass flows are visualized in Figure 17c and Table 5.

The results obtained according to Figure 18 show a comparison of the three different modes of use with respect to the real solar radiation. In variable mode, a usage time of 16.25 h is obtained. Mode 0 (economical) will maintain a time of use of 17.55 h, but at the lowest cooling power of 3 kW. Finally, Mode 5 (greater power) is maintained at a time of use of 14.86 h with the maximum cooling power of 5 kW. This mode is the one that has the least time of use.

Table 5. Different modes of operation varying in time for radiation of 900 kW/m².

Time (h)	Mode	Power (kW)	Mass Flow \dot{m}_g (kg/s)	Mass Flow \dot{m}_e (kg/s)
0	0	3.075–3.11	0.0347–0.035	0.0189–0.0191
1.5	1	3.245–3.287	0.0365–0.037	0.0199–0.0202
1.8	2	4.2388	0.0478	0.0261
2.3	3	4.87–4.905	0.0549–0.0552	0.0299–0.0301
4.9	5	4.87–4.905	0.0549–0.0552	0.0299–0.0301
4.3	3	4.87–4.905	0.0549–0.0552	0.0299–0.0301
4.9	2	4.2388	0.0478	0.0261
5.8	1	3.245–3.287	0.0365–0.037	0.0199–0.0202
6.8	0	3.075–3.11	0.0347–0.035	0.0189–0.0191

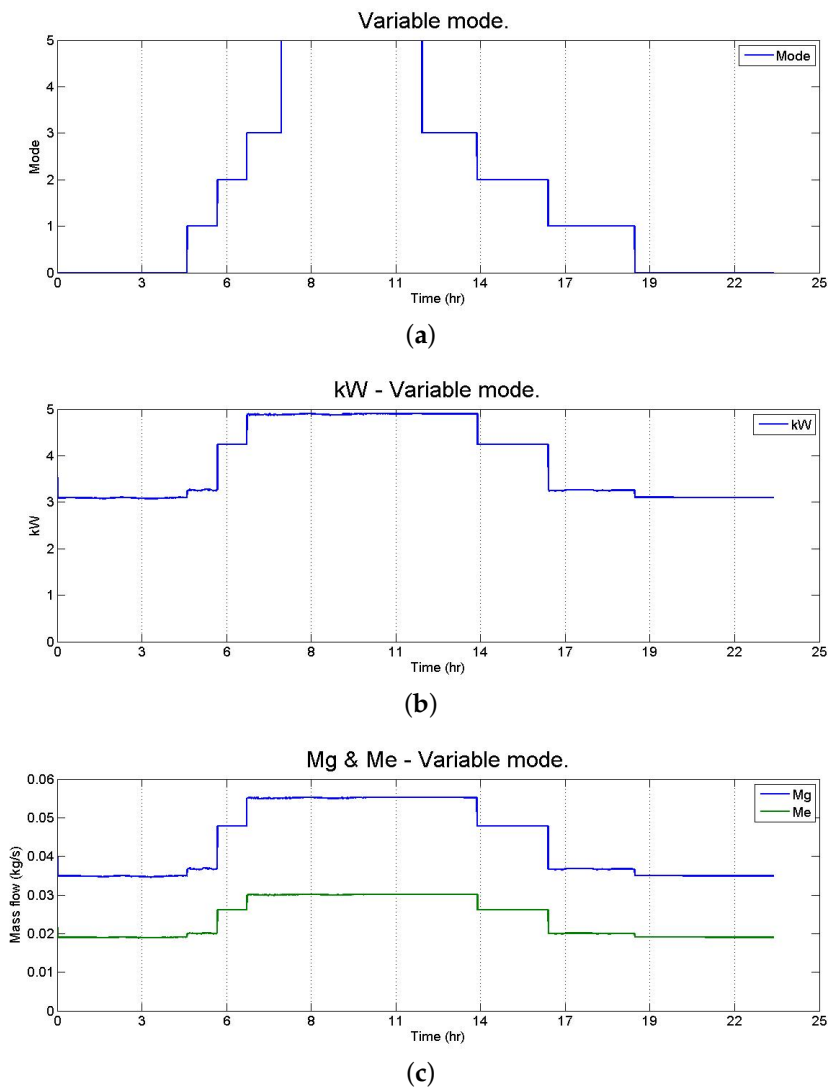


Figure 17. Behavior of the variable mode of use of the cooling system defined by the end user. (a) Variable mode used. (b) kW of variable mode. (c) Mass flow for the generator and evaporator.

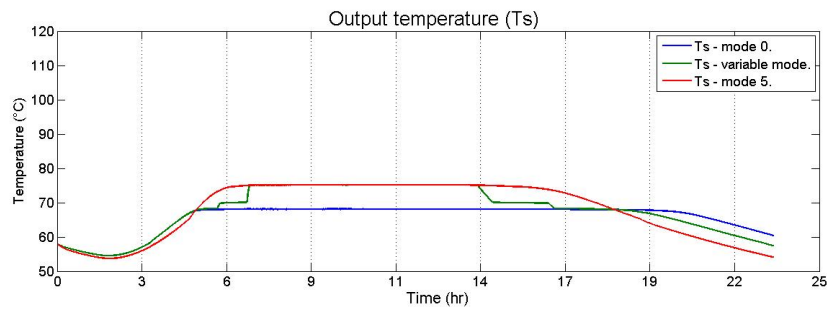


Figure 18. Comparison of the generator temperature of the three modes of operation with a solar radiation of 900 kW/m^2 .

5.2. Disturbed Radiation

A series of simulations is performed to analyze different modes of operation with a solar radiation of 500 kW/m^2 considered as low radiation, which starts from 7:00 a.m. and ends around 7:00 p.m., as shown in Figure 13b.

The first simulation test with a perturbed radiation is for Mode 0; according to Figure 19a, the collector reaches an approximate temperature of $85 \text{ }^\circ\text{C}$, and the reference temperature $T_{s(ref)}$ is kept constant at $68 \text{ }^\circ\text{C}$. On the other hand, Mode 5, as shown in Figure 19b, reaches a collector temperature of over $80 \text{ }^\circ\text{C}$ with a reference temperature $T_{s(ref)}$ of $75 \text{ }^\circ\text{C}$ required. The variable mode reaches a collector temperature of $85 \text{ }^\circ\text{C}$, and the reference temperature varies at two different temperatures, starting with $68 \text{ }^\circ\text{C}$; after 7.5 h, it reaches $70 \text{ }^\circ\text{C}$; passing 4.5 h, the reference temperature drops from $70\text{--}68 \text{ }^\circ\text{C}$; during 8.7 h, it stays constant until the day is over. This is the behavior of variable mode, as shown in Figure 19c.

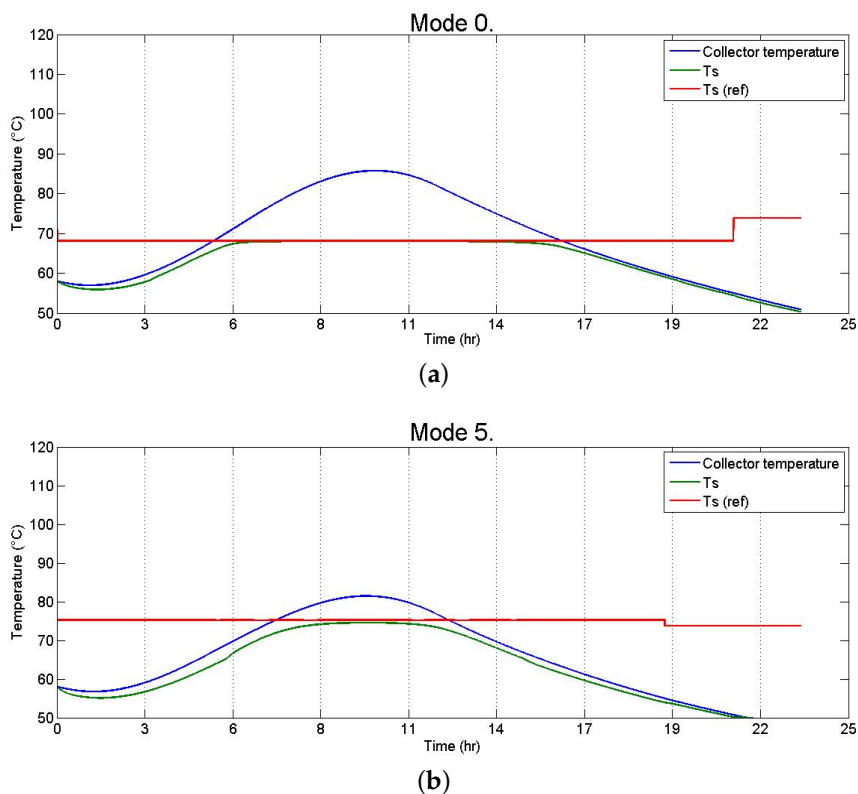


Figure 19. Cont.

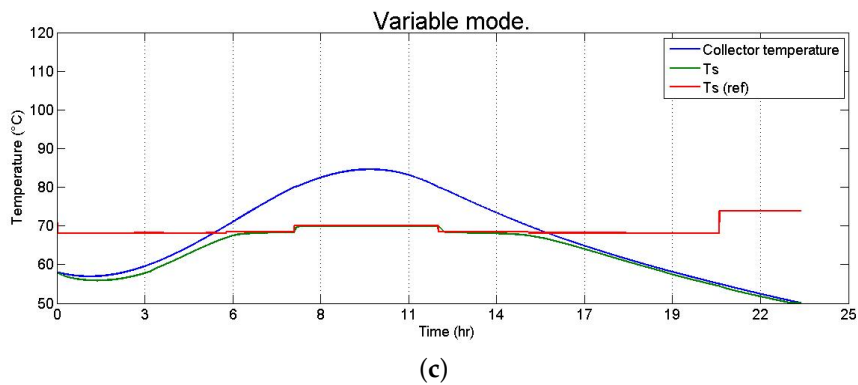


Figure 19. Analysis for different modes of operation with a solar radiation of 500 kW/m^2 , which is considered low radiation. (a) Test for Mode 0; (b) Mode 5; (c) variable mode.

For Modes 0 and 5, the cooling capacities are shown in Figure 20. For Mode 0, a capacity of 3 kW is needed. For Mode 5, its cooling capacity is 5 kw. The variable mode is shown in Figure 21; the modes operate from 0–2, as shown in Figure 21a. The power varies according to the solar radiation, as shown in Figure 21b.

The mass flow of the generator and evaporator for Modes 0 and 5 is shown in Table 6 and Figure 22. For variable mode, different powers and mass flows are visualized in Table 7; Figure 21c shows the behavior of the evaporator and generator flow for variable mode, which is perceived to have the same behavior and operating times, but with different flows.

Finally, a comparison is made for the three modes of use with a solar radiation of 500 kW/m^2 according to Figure 23. In variable mode, it is obtained with a use time of 11.5 h. Mode 0 (economical) maintain a time of use of 11.93 h at the lowest cooling power of 3 kW. Mode 5 (greater power) is maintained with a use time of 9.5 h; with the maximum cooling power of 5 kW, the use time is the lowest compared with the two previous modes.

Table 6. Comparison of the economic mode and the maximum mode for a radiation of 500 kW/m^2 .

Mode of Use	Power (kW)	Mass Flow \dot{m}_g (kg/s)	Mass Flow \dot{m}_e (kg/s)	Time (h)
Economic mode (Mode 0)	3	0.035	0.018	11.93
Maximum mode (Mode 5)	5	0.0548–0.0553	0.0299–0.0301	9.5

Table 7. Behavior of the variable mode for a radiation of 500 kW/m^2 .

Time (h)	Mode	Power (kW)	Mass Flow \dot{m}_g (kg/s)	Mass Flow \dot{m}_e (kg/s)
0	0	3.075–3.108	0.0347–0.035	0.0189–0.0191
1.9	1	3.245–3.265	0.0365–0.037	0.0199–0.0202
2.7	2	4.2388	0.0478	0.0261
4.3	1	3.245–3.2655	0.0365–0.0368	0.0199–0.0201
5.4	0	3.075–3.108	0.0347–0.035	0.0189–0.0191

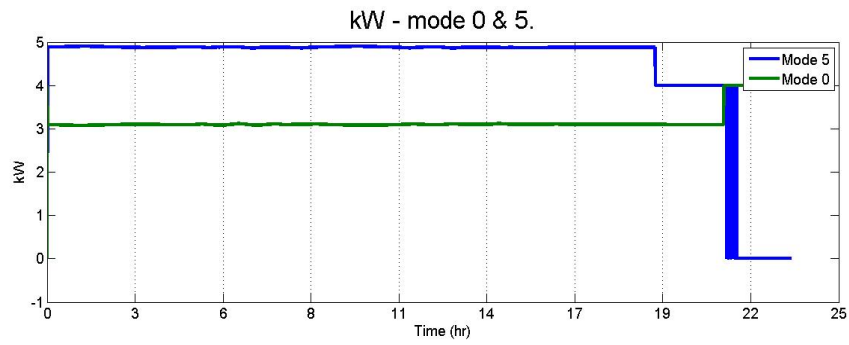


Figure 20. Cooling capacity for Modes 0 and 5.

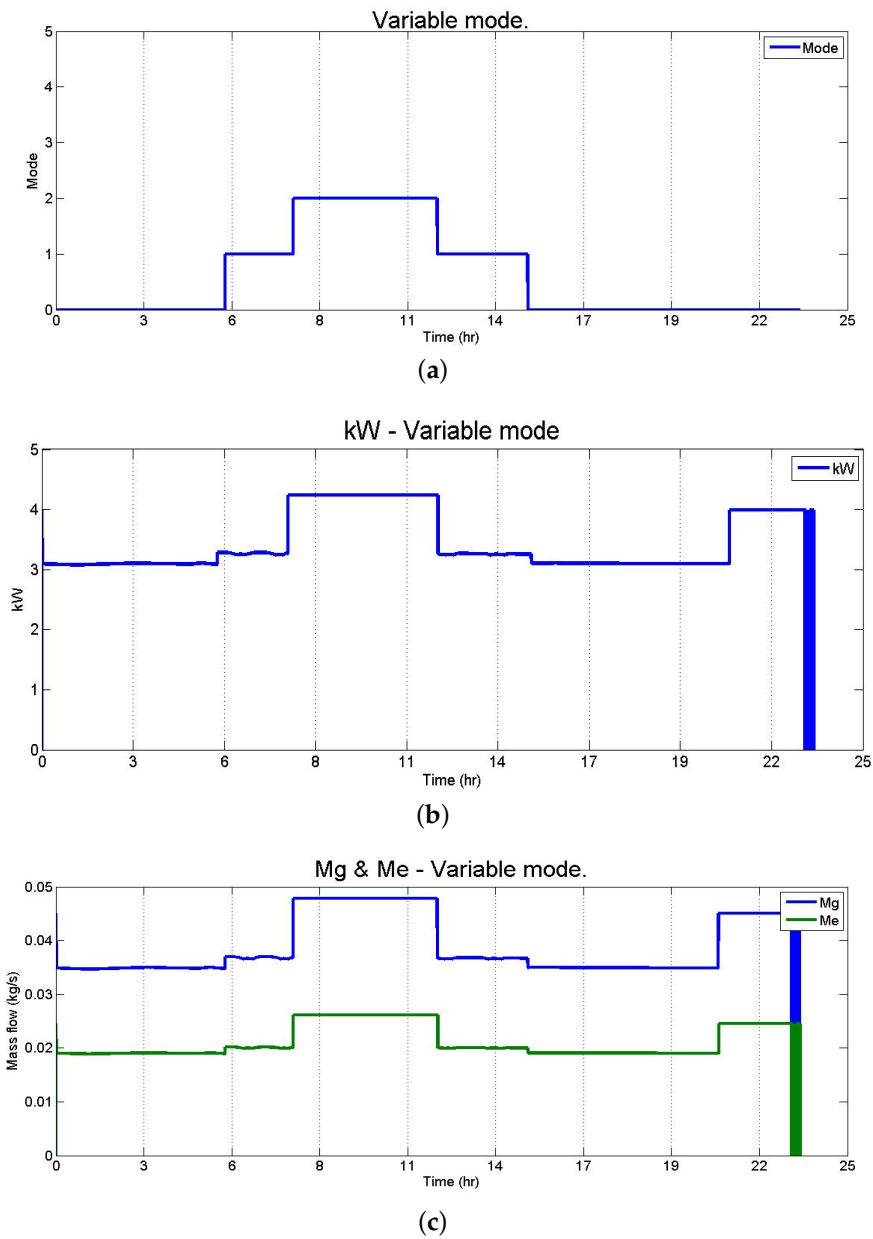


Figure 21. Behavior of the variable mode of use of the cooling system defined by the end user for a radiation of 500 kW/m^2 . (a) Variable mode used; (b) kW of the variable mode; (c) mass flow for the generator and evaporator.

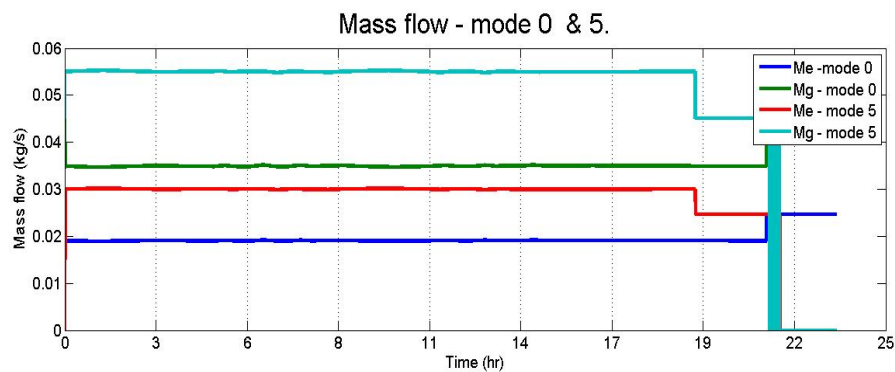


Figure 22. Mass flow for Modes 0 and 5.

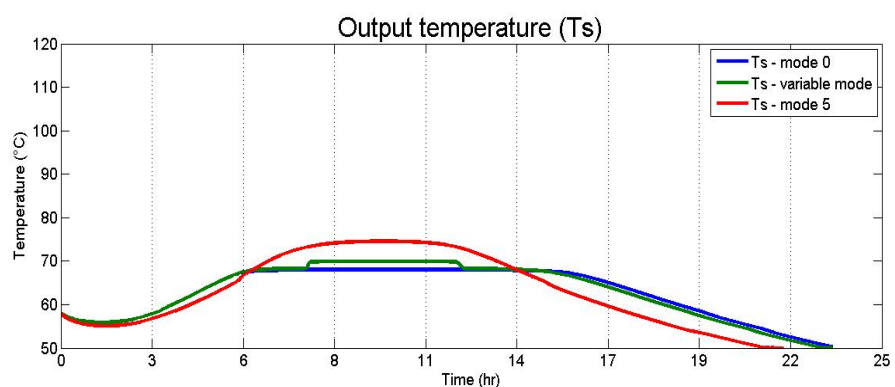


Figure 23. Comparison of the generator temperature of the three modes of operation with a solar radiation of 500 kW/m^2 .

6. Conclusions

The analysis and design of a control system that optimizes the time of use in a solar-assisted air-conditioning system were accomplished in this work. The main objective is to optimize the refrigeration cycle by an ejector for a solar air-conditioning system, using a single controller, optimizing physical resources and minimizing operating and maintenance costs. The priority is to increase the time of use of a solar air-conditioning system, thus facilitating its implementation, maintenance and easy development.

A control structure based on two layers was designed. The first layer implements a temperature-control system of a storage tank, which follows a reference defined by a supervisory control layer. The second layer is supervisory control and optimization, which automatically generates a series of references for better performance of the air-conditioning. These references take into account solar-power supply conditions, user-defined modes of operation and disturbances of the system, thus optimizing the cost function based on the longest possible time of use. The advantage of this concept is being able to perform the optimization easily for a set of operation modes in the same refrigeration cycle controlled by the same controller, in spite of unknown dynamics and perturbations. Three simulations with different modes of operation are analyzed; the first mode of operation, called Mode 0, is the most economical; the second mode of operation, called Mode 5, is the least economical, but has higher cooling power; and lastly, variable mode is performed, in which cooling capacity depends on the selection of functioning modes by the end users.

The simulations show that a fuzzy governor control can be optimized to obtain better performance in terms of time of use of a solar thermal system for residential applications. The operating tests prove that a time of use of approximately 17.55 h can be obtained in an optimized mode of operation in power economy. However, without an optimized control system and at the same conditions of

functionality, solar air-conditioning would only work approximately for 14.85 h, in the case of a single point of operation, for which it was designed. Fuzzy intelligent controls and optimization systems were compared for a typical operating day, with real and simulated solar radiation, showing that it is possible to improve the performance and reliability of nonlinear solar thermal systems in several ways:

- Greater scalability, facilitating different operation points in an ejector-based refrigeration cycle, without the need for reconfiguring the system.
- Increased usage time of a solar air-conditioning system, thus facilitating their implementation, maintenance and easy development.
- Different tests show that the intelligent optimization and control systems are self-adapting to the end user requirements, disturbances and climatic conditions.
- Less human supervision required.
- No need to use electrical installations for the operation and use of solar air-conditioning.
- Lower cost of implementation, maintenance and nonrenewable energy consumption.

Finally, the tests performed demonstrate that the designed control structure optimizes the time of use before different conditions, the selection of functioning modes by end users, disturbances and solar radiation.

Acknowledgments: This work has been supported by University of Colima (Mexico), Agrobiotechnology Laboratory of University of Colima (Area: Automation, Instrumentation, and Control) and the National Council for Science and Technology (CONACYT) of the Mexican Republic, with support for the high-quality graduate program, Announcement 15_3_2015_1_1 and Reference 005016.

Author Contributions: Giovanna Avedian-González, Apolinar González-Potes, Vrani Ibarra-Junquera, Walter A. Mata-López and Carlos Escobar-del Pozo jointly contributed to the design of the control strategy, simulations, data analysis and writing of the paper.

Conflicts of Interest: The authors declare no conflict of interest.

References

1. Dai, Y.J.; Wang, R.Z.; Zhang, H.F.; Yu, J.D. Use of liquid desiccant cooling to improve the performance of vapor compression air-conditioning. *Appl. Therm. Eng.* **2001**, *21*, 1185–1202.
2. Hermes, C.J.; Melo, C.; Knabben, F.T.; Gonçalves, J.M. Prediction of the energy consumption of household refrigerators and freezers via steady-state simulation. *Appl. Energy* **2009**, *86*, 1311–1319.
3. Vereda, C.; Ventas, R.; Lecuona, A.; Venegas, M. Study of an ejector-absorption refrigeration cycle with an adaptable ejector nozzle for different working conditions. *Appl. Energy* **2012**, *97*, 305–312.
4. Salata, F.; Tarsitano, A.; Golasi, I.; de Lieto Vollaro, E.; Coppi, M.; de Lieto Vollaro, A. Application of absorption systems powered by solar ponds in warm climates for the air-conditioning in residential buildings. *Energies* **2016**, *9*, 821.
5. Gassar, A.A.A.; Yun, G.Y. Energy Saving Potential of PCMs in Buildings under Future Climate Conditions. *Appl. Sci.* **2017**, *7*, 1219.
6. Coulomb, D.; Dupon, J.L.; Pichard, A. The Role of Refrigeration in the Global Economy. In *29th Informatory Note on Refrigeration Technologies*; Technical Report; International Institute of Refrigeration: Paris, France, 2015.
7. Romano, R.; Siano, P.; Acone, M.; Loia, V. Combined Operation of Electrical Loads, Air Conditioning and Photovoltaic-Battery Systems in Smart Houses. *Appl. Sci.* **2017**, *7*, 525.
8. Moo-Yeon, L. Design and Cooling Performances of an Air Conditioning System with Two Parallel Refrigeration Cycles for a Special Purpose Vehicle. *Appl. Sci.* **2017**, *7*, 190.
9. Yang, L.; Yan, H.; Lam, J.C. Thermal comfort and building energy consumption implications: A review. *Appl. Energy* **2014**, *115*, 164–173.
10. Isaac, M.; van Vuuren, D.P. Modeling global residential sector energy demand for heating and air-conditioning in the context of climate change. *Energy Policy* **2009**, *37*, 507–521.
11. Henning, H.; Döll, J. Solar Systems for Heating and Cooling of Buildings—1st International Conference on Solar Heating and Cooling for Buildings and Industry (SHC 2012). *Energy Procedia* **2012**, *30*, 633–653.

12. Reda, F.; Viot, M.; Sipilä, K.; Helm, M. Energy assessment of solar cooling thermally driven system configurations for an office building in a Nordic country. *Appl. Energy* **2016**, *166*, 27–43.
13. Dale, M. A Comparative Analysis of Energy Costs of Photovoltaic, Solar Thermal, and Wind Electricity Generation Technologies. *Appl. Sci.* **2013**, *3*, 325–337.
14. Khattab, N.M.; Barakat, M.H. Modeling the design and performance characteristics of solar steam-jet cooling for comfort air-conditioning. *Solar Energy* **2002**, *73*, 257–267.
15. Huang, B.J.; Petrenko, V.A.; Samofatov, I.Y.; Shchetinina, N.A. Collector selection for solar ejector cooling system. *Solar Energy* **2001**, *71*, 269–274.
16. Wolpert, J.L.; Riffat, S.B. kW cooling hybrid solar/gas ejector air-conditioning system. In Proceedings of the 1st International Conference on Sustainable Energy Technologies, 2002.
17. Balaras, C.A.; Grossman, G.; Henning, H.M.; Ferreira, C.A.I.; Podesser, E.; Wang, L.; Wiemken, E. Solar air-conditioning in Europe—An overview. *Renew. Sustain. Energy Rev.* **2007**, *11*, 299–314.
18. Henning, H.M. Solar assisted air-conditioning of buildings: An overview. *Appl. Therm. Eng.* **2007**, *27*, 1734–1749.
19. Daou, K.; Wang, R.Z.; Xia, Z.Z. Desiccant cooling air-conditioning: A review. *Renew. Sustain. Energy Rev.* **2006**, *10*, 55–77.
20. Rafique, M.M.; Rehman, S.; Alhems, L.M.; Lashin, A. Parametric Analysis of a Rotary Type Liquid Desiccant Air Conditioning System. *Energies* **2016**, *9*, 305.
21. Nguyen, V.M.; Riffat, S.B.; Doherty, P.S. Development of a solar-powered passive ejector cooling system. *Appl. Therm. Eng.* **2001**, *21*, 157–168.
22. Hong, H.; Guohui, F.; Hongwei, W. Performance research of solar hybrid desiccant cooling systems. *Procedia Environ. Sci.* **2012**, *12*, 57–64.
23. Romero Paguay, J.A.; Carbonell Morales, T.; Tumailli, Q.; Fernanda, V. Simulación de un sistema de refrigeración solar por absorción. *Ing. Energ.* **2016**, *37*, 154–162. (In Galician)
24. Huang, B.J.; Chang, J.M.; Petrenko, V.A.; Zhuk, K.B. A solar ejector cooling system using refrigerant R141b. *Sol. Energy* **1998**, *64*, 223–226.
25. Rusly, E.; Aye, L.; Charters, W.W.S.; Ooi, A. CFD analysis of ejector in a combined ejector cooling system. *Int. J. Refrig.* **2005**, *28*, 1092–1101.
26. Amigo, M.L.; Vergel, O.A. *FriO Industrial y Aire Acondicionado*; Universidad de Castilla La Mancha: Ciudad Real, Spain, 2012. (In Spanish).
27. Bujedo, L.A.; Rodríguez, J.; Martínez, P.J. Experimental results of different control strategies in a solar air-conditioning system at part load. *Sol. Energy* **2011**, *85*, 1302–1315.
28. Rosiek, S.; Garrido, F.J.B. Performance evaluation of solar-assisted air-conditioning system with chilled water storage (CIESOL building). *Energy Convers. Manag.* **2012**, *55*, 81–92.
29. Ferhatbegović, T.; Palensky, P.; Fontanella, G.; Basciotti, D. Modelling and design of a linear predictive controller for a solar powered HVAC system. In Proceedings of the 2012 IEEE International Symposium on Industrial Electronics, Hangzhou, China, 28–31 May 2012; pp. 869–874.
30. Sousa, J.M.; Babuška, R.; Verbruggen, H.B. Fuzzy predictive control applied to an air-conditioning system. *Control Eng. Pract.* **1997**, *5*, 1395–1406.
31. Herrera, E.; Bourdais, R.; Guéguen, H. Predictive and interactive controllers for solar absorption cooling systems in buildings. *J. Process Control* **2014**, *24*, 836–845.
32. Garcia-Gabin, W.; Zambrano, D.; Camacho, E.F. Sliding mode predictive control of a solar air-conditioning plant. *Control Eng. Practice* **2009**, *17*, 652–663.
33. Ferhatbegović, T.; Zucker, G.; Palensky, P. Model based predictive control for a solar-thermal system. In Proceedings of the 10th IEEE AFRICON, Livingstone, Zambia, 13–15 September 2011; pp. 1–6.
34. Sonntag, C.; Ding, H.; Engell, S. Supervisory control of a solar air-conditioning plant with hybrid dynamics. *Eur. J. Control* **2008**, *14*, 451–463.
35. Kang, C.S.; Park, J.I.; Park, M.; Baek, J. Novel modeling and control strategies for a HVAC system including carbon dioxide control. *Energies* **2014**, *7*, 3599–3617.
36. Ma, X.; Zhang, W.; Omer, S.A.; Riffat, S.B. Experimental investigation of a novel steam ejector refrigerator suitable for solar energy applications. *Appl. Therm. Eng.* **2010**, *30*, 1320–1325.
37. Yapıcı, R.; Akkurt, F. Experimental investigation on ejector cooling system performance at low generator temperatures and a preliminary study on solar energy. *J. Mech. Sci. Technol.* **2012**, *26*, 3653–3659.

38. Sripanom, C.; Vaivudh, S. *Performance of R141b Ejector with Thermal Storage for Solar Air Conditioning*; Editorial Board Members; Elsevier: Amsterdam, The Netherlands, 2015; p. 784.
39. Varga, S.; Oliveira, A.C.; Diaconu, B. Analysis of a solar-assisted ejector cooling system for air-conditioning. *Int. J. Low-Carbon Technol.* **2009**, *4*, 2–8.
40. Sun, D.W. Comparative study of the performance of an ejector refrigeration cycle operating with various refrigerants. *Energy Convers. Manag.* **1999**, *40*, 873–884.
41. Huang, B.J.; Chang, J.M.; Wang, C.P.; Petrenko, V.A. A 1-D analysis of ejector performance. *Int. J. Refrig.* **1999**, *22*, 354–364.
42. Varga, S.; Oliveira, A.C.; Diaconu, B. Numerical assessment of steam ejector efficiencies using CFD. *Int. J. Refrig.* **2009**, *32*, 1203–1211.
43. Chaiwongsa, P.; Wongwiset, S. Experimental study on R-134a refrigeration system using a two-phase ejector as an expansion device. *Appl. Therm. Eng.* **2008**, *28*, 467–477.
44. Khalil, A.; Fatouh, M.; Elgendy, E. Ejector design and theoretical study of R134a ejector refrigeration cycle. *Int. J. Refrig.* **2011**, *34*, 1684–1698.
45. Kumar, J.; Jain, N. Performance Analysis of Heat Operated Ejector Refrigeration System with Natural Refrigerants R-717 and Propane. *Int. J. Sci. Res.* **2013**, *2*, 139–141.
46. Dong, J.; Chen, X.; Wang, W.; Kang, C.; Ma, H. An experimental investigation of steam ejector refrigeration system powered by extra low temperature heat source. *Int. Commun. Heat Mass Transfer.* **2017**, *81*, 250–256.
47. Selvaraju, A.; Mani, A. Experimental investigation on R134a vapour ejector refrigeration system. *Int. J. Refrig.* **2006**, *29*, 1160–1166.
48. Selvaraju, A.; Mani, A. Analysis of an ejector with environment friendly refrigerants. *Appl. Therm. Eng.* **2004**, *24*, 827–838.
49. Cengel, Y.A.; Boles, M.A. *Thermodynamics: An Engineering Approach*. Available online: <https://www.amazon.com/Thermodynamics-Engineering-Approach-Yunus-Cengel/dp/0072383321> (accessed on 2 February 2018).
50. Rodríguez-Hidalgo, M.C.; Rodríguez-Aumente, P.A.; Lecuona, A.; Gutiérrez-Urueta, G.L.; Ventas, R. Flat plate thermal solar collector efficiency: Transient behavior under working conditions. *Part I Model Descr. Exp. Valid.* **2011**, *31*, 2394–2404.
51. Arora, S.; Chitkara, S.; Udayakumar, R.; Ali, M. Thermal analysis of evacuated solar tube collectors. *J. Pet. Gas Eng.* **2011**, *4*, 74–82.



© 2018 by the authors. Licensee MDPI, Basel, Switzerland. This article is an open access article distributed under the terms and conditions of the Creative Commons Attribution (CC BY) license (<http://creativecommons.org/licenses/by/4.0/>).